Measurements of Jet Production in Deep Inelastic Scattering

Leif Jönsson

Phys. Dept., Lund University, Box 118, 221 00 Lund, Sweden

Abstract. Some recent results based on jet production at the HERA ep-collider are presented. Inclusive jet cross sections have proven to be in good agreement with predictions from QCD Monte Carlo models up to very high momentum transfer whereas di-jet cross sections are less well described. Recent next-to-leading order calculations turn out to reproduce the di-jet data very well which enables a direct determination in next-to-leading order of the gluon density in the proton and an improved measurement of the strong coupling constant.

1 Introduction

Considerable progress in our understanding of how matter is constructed has been made over the past decades mainly thanks to results from deep inelastic scattering (DIS) experiments. The basic idea behind these experiments dates as far back as to Rutherford's famous experiment from 1911 in which it was proven that the atom contains a massive nucleus. In modern experiments leptons are used to probe the structure of matter, the advantage being that the leptons, as far as we know, are pointlike particles and that their interaction with matter can be described by a well founded theory, the electroweak theory. The basic DIS process (zeroth order in QCD) is a purely electroweak interaction between a highly virtual photon emitted by the incoming lepton and a parton in the proton (Fig. 1a).

The HERA storage ring, which collides 27.5 GeV positrons (electrons) with 820 GeV protons, has provided a great increase in resolution by extending the accessible kinematic range by several orders of magnitude in the transverse momentum squared, Q^2, transferred by the virtual photon and in the Bjorken scaling variables, x and y.

The scattered electron from a DIS process carries information about the parton density in the proton as does also the particle jet from the scattered quark, which is usually called the current jet. Thus an inclusive measurement of either the scattered electron or the current jet will determine the proton structure function, F_2. Results from HERA have revealed a steep rise of the structure function as the fractional parton momentum decreases. This can be explained by a model where the emitted gluons split up into quark-antiquark pairs and thus create a large number of sea-quarks. The more partons sharing the proton momentum the less fraction each of them will carry. Since the gluons are driving the strong rise via the sea-quarks the gluon density can

be determined from the proton structure function assuming that the QCD splitting functions describing the parton emission are correct.

A more direct determination of the gluon density would be to measure the rate of boson-gluon fusion (BGF) processes, which is of first order in the strong coupling constant, α_S. The BGF process is an interaction between the virtual photon and a gluon which has fragmented into a quark-antiquark pair (Fig. 1c) and consequently the final state will contain two hard jets. Another first order α_S process is QCD-Compton scattering where a gluon is emitted from the scattered quark (Fig. 1b). Being of first order in α_S, both processes are thus sensitive to the strong coupling constant and can be used to determine its value. Even though the di-jet cross section is proportional to α_S, leading order (LO) calculations leave the renormalization scale undetermined. Thus higher order corrections are necessary to reduce the dependence of the cross section on the renormalization (μ_r) and factorization (μ_f) scales. It turns out that already NLO corrections leads to much smaller dependences on μ_r and μ_f which make reliable cross section calculations possible. In recent years several Monte Carlo programs, like MEPJET [1], DISENT [2] and DISASTER++ [3], have been developed, providing cross sections calculations on the parton level and allowing for the application of various kinematic cuts and choices of jet algorithms. In order to cancel infrared divergencies which appear in the analytic calculations due to soft or collinear gluon emissions two methods have been used. The MEPJET program uses the phase space slicing method [4] which requires the matrix elements for the real emission process to be approximated in the regions close to the singularities. These regions are defined by the introduction of non-physical cut-off parameters. The DISENT program is based on the subtraction method [5] which uses the exact matrix element expression in the whole phase space region. In this method the singularities due to soft and collinear gluon emission will explicitely cancel against the poles in the virtual diagrams.

Since the cross section for di-jet production at HERA energies is in the range 100 pb to few nb, enough statistics will be available for various precision tests of QCD.

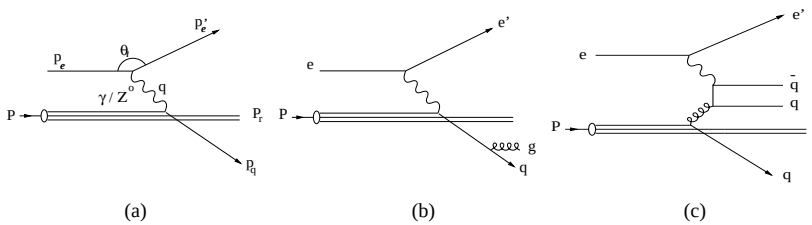

Fig. 1. Generic Feynman diagrams for zeroth and first order α_S processes.

The kinematics of a deep inelastic scattering event can be determined from two independent Lorentz variables, which can be any of the two Bjoerken scaling variables x or y, the square of the momentum, Q^2, transferred by the exchanged boson and the invariant mass squared of the hadronic system, W^2. These variables are defined in terms of the 4-momenta of the incoming proton, P, the incoming and scattered electron, p_e and p'_e, and of the virtual boson, q.

$$Q^2 \equiv -q^2 = -(p_e - p'_e)^2 \tag{1}$$

$$y \equiv \frac{P \cdot q}{P \cdot p_e} \tag{2}$$

$$x \equiv \frac{-q^2}{2P \cdot q} = \frac{Q^2}{ys} \tag{3}$$

$$W^2 \equiv (q+P)^2 = Q^2 \left(\frac{1-x}{x}\right) + m_p \tag{4}$$

where m_p is the mass of the proton.

Other variables which are useful in describing the kinematic properties of di-jet events are the Lorentz invariant partonic scaling variables x_p and z_p.

$$x_p = \frac{Q^2}{2p \cdot q} = \frac{Q^2}{2\xi P \cdot q} = \frac{x}{\xi} \approx \frac{Q^2}{Q^2 + \hat{s}} \tag{5}$$

$$z_p = \frac{P \cdot p_{jet}}{P \cdot q} \approx \frac{E_{jet}(1 - cos\theta_{jet})}{\sum_i E_i(1 - cos\theta_i)} \tag{6}$$

where ξ is the fraction of the proton momentum carried by the interacting parton and $\hat{s}$ is the invariant mass squared of the hard subsystem. E_{jet} and θ_{jet} are the energy and polar angle of the jet whereas E_i and θ_i are the energy and polar angle of the individual hadrons in the hard subsystem.

The first order parton level process must be corrected for higher order perturbative QCD effects causing the emission of additional partons on a short space-time scale before hadronisation. For example the LEPTO [6] and HERWIG [7] event generators calculate processes up to the first order in α_S by using exact QCD matrix elements convulated with the parton densities in the proton. Additional parton emission is generated using the DGLAP [8] equations in a so called parton shower evolution. In the ARIADNE [9] Monte Carlo program gluons are emitted due to the colour dipole model [10] from independently radiating colour dipoles which are stretched between the partons.

Due to the bremsstrahlung nature of this radiation, most partons will be soft or collinear with the emitting parton and will thus not produce separately observable jets, but rather cause softening of the hadron momenta and broadening of the jet. The reconstruction of a jet must therefore account correctly for both the parton emission process and the hadronisation process.

There are different approaches to describe the fragmentation of partons into hadrons. The most naive picture is to assume that the different partons fragment independently (*independent fragmentation* [11]). This model is, however, connected with several problems like non-conservation of the total flavour, energy and momentum, and it is also not Lorentz invariant. In the *string fragmentation* [12] picture a colour flux tube is streched between a quark and an antiquark. If the transverse dimensions of the tube is assumed to be uniform along its length, this automatically leads to confinement with a linearly rising potential. In case a gluon is emitted the colour string will be streched from the quark via the gluon to the antiquark and if several gluons are emitted the string picture becomes correspondingly more complicated. As the partons move apart the energy stored in the string will increase and eventually it will break up creating new quark antiquark pairs. The Lund string fragmentation is for example used in the LEPTO and ARIADNE programs. The concept of *cluster fragmentation* [13] contains three components. The generation of clusters by parton shower evolution, the fragmentation of large clusters into smaller ones, and the decay of clusters into hadrons. The clusters are assumed to be the basic units from which hadrons are produced. The decay is assumed to be isotropic in the rest frame of the cluster which gives a compact description with few parameters. This fragmentation model is used by the HERWIG generator.

The intuitive picture of a jet as a collimated flow of particles implies that a minimum energy must be available for the jet formation. In particular, the particle momenta along the initial parton direction must be much larger than the transverse momentum fluctuations induced in the hadronisation process. As the parton momentum increases, the jets tend to be more collimated which simplifies their identification. Nevertheless, the definition of a jet is not unambigous.

A number of jet-finding algorithms have been developed to provide ways of reconstructing jets but since the definition of a jet is not unique, the algorithms all include a parameter which specifies the desired resolution. The input to a jet algorithm are 4-vectors representing particles and/or energy clusters in the detector and as output the 4-momenta of the jets are given. If the resolution depends on the kinematic region in which the algorithm is applied, a suitable scaling variable has to be found to account for this kinematic dependence.

There are two general types of jet algorithms. The *cone algorithms* [14] are based on the definition of a cone with its tip in the interaction point and with a predefined opening angle, normally defined through $R = \sqrt{\eta^2 + \phi^2}$, where η is the pseudorapidity and ϕ the azimuthal angle. The cone is swept over the solid angle covered by the detector and a jet is defined by maximizing the total energy inside the cone. The *cluster algorithms* calculate the distances between pairs of particles or energy clusters using some distance parameter which is specific to each algorithm. In an iterative process such

pairs are merged until the distance parameter exceeds a predefined cut-off value, specifying the resolution of the algorithm. The jet algorithms which will be mentioned here are two versions of the k_T algorithm and the modified Durham algorithm, which are all cluster algorithms. The factorizable k_T algorithm [15] uses two distance parameters to determine whether a particle should be merged with another particle or with the proton remnant which is represented by an infinite momentum particle. The distance parameters are defined as $k^2_{T,ij} = 2min(E^2_i, E^2_j)(1-cos\theta_{ij})$ and $k^2_{T,ir} = 2E^2_i(1-cos\theta_{ir})$, where i and j represents particles and r the proton remnant. The longitudinally invariant k_T algorithm [16] uses the same procedure but with cone like distance parameters; $k^2_{T,ij} = 2min(E^2_{T,i}, E^2_{T,j})(\Delta\eta^2_{ij} + \Delta\phi^2_{ij})$ and $k^2_{T,ir} = 2E^2_{T,i}$ The modified Durham algorithm is a modification of the JADE algorithm [17] with one distance parameter, $k^2_{T,ij} = 2min(E^2_i, E^2_j)(1 - cos\theta_{ij})$. The cut-off parameter is scaled with W^2.

2 Inclusive jet cross sections

The production of multi-jet events at high Q^2 can be used to test the predictions by perturbative QCD. The ZEUS collaboration has used a data sample corresponding to $42.5pb^{-1}$ to study inclusive jet production. The jets were reconstructed in the laboratory system using the longitudinally invariant k_T algorithm on clusters in the calorimeter. Reconstructed jets were required to have a transverse momentum greater 14 GeV and only jets within the pseudorapidity range $-1 < \eta < 2$ were accepted since this is the region where the calorimeter offers good acceptance. As an example of the comparisons between data and QCD models the differential jet cross section $d\sigma/dQ^2$ is shown in fig 2a and b. It is seen that ARIADNE describes the data very well up to the highest Q^2 bin where a slight deviation can be observed. This is, however, probably due to the fact that the version of ARIADNE which was used doesn't give a proper description of the jet cross sections at high Q^2. It should also be kept in mind that since the jet reconstruction has been performed in the laboratory frame the tranverse energies of the jets are strongly influenced by event kinematics. Further the event sample is dominated by zeroth order α_S events and therefore the sensitivity to QCD effects is suppressed.

3 A direct determination of the gluon density in NLO

A direct determination of the gluon density is not only motivated by its own interest but a comparison with indirect measurements constitutes an important test of QCD. The lack of cross section calculations to next-to-leading order restricted an earlier analysis to a LO determination [18]. Since then several NLO programs, which can be applied for various jet algorithms and

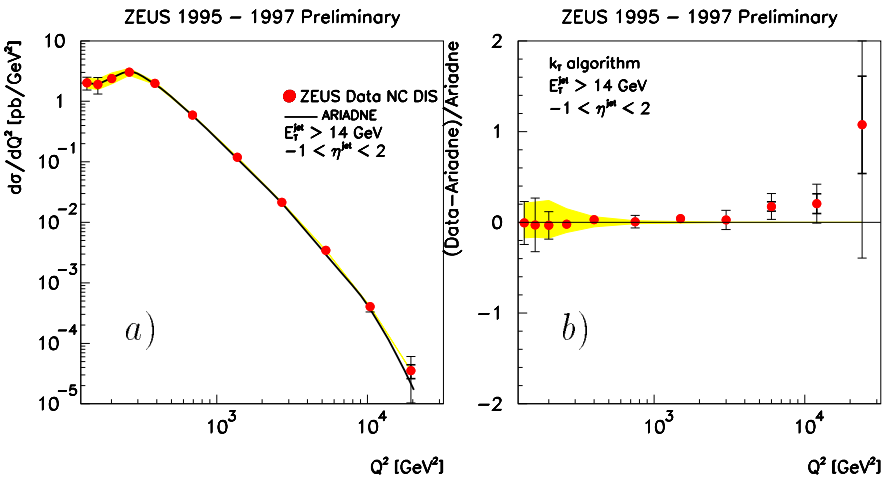

Fig. 2. The differential inclusive jet cross section $d\sigma/dQ^2$ compared to the predictions by ARIADNE.

experimental cuts, have become available. Although the QCD-Compton process has the same event topology as the BGF process and thus constitutes a background, the BGF process dominates in the kinematic region investigated.

A recent H1 analysis was based on an integrated luminosity of 36 pb^{-1} collected in the years 1994-97. It was performed in a kinematic region which covers a wide range in the transverse momentum transfer squared, $10 < Q^2 < 5000 GeV^2$, and was restricted to $0.2 < y < 0.6$ in order to get a good determination of y from the measurement of the scattered electron and to suppress backgrounds from photoproduction processes. The jet reconstruction was performed in the Breit frame using the longitudinally invariant k_T algorithm, since this turns out to give the smallest hadronisation corrections, as determined from Monte Carlo models. The jets were required to have a transverse energy sum, $E_{T,jet1} + E_{T,jet2}$, greater than 17 GeV in the Breit frame and simultaneously the transverse energy of each jet had to be greater than 5 GeV. With the additional cut $-1 < \eta_{jet} < 2.5$ in the laboratory system, it was ensured that the jets were well inside the hadronic calorimeter. The data were corrected for detector effects and initial and final state electroweak radiation by performing detailed simulations using DJANGO [19] which provides an interface between the ARIADNE and LEPTO events generators, repectively and HERACLES [20].

Since hadronisation corrections are small the data has been compared directly to NLO calculations performed with the DISENT program, using the CTEQ5M [21] parton density parametrization and its corresponding α_S value of 0.116. The factorization scale was chosen to be $\mu_f^2 = 200 GeV^2$, which is approximately equal to the average transverse energy squared of

the jets in the Breit frame. Q^2 was taken as the renormalisation scale, μ_r. Fig. 3a shows the corrected differential cross section as a function of the jet scattering angle, defined as $\eta' = \frac{\eta_{1,Breit} - \eta_{2,Breit}}{2}$, for three regions in $E_{T,Breit}$ of the jets. The agreement between the data and the NLO predictions is good and it can be observed that the jet production at larger angles is suppressed as E_T increases. In Fig. 3b the differential cross section is plotted against the fractional parton momentum, ξ, in four different Q^2 bins for comparisons of the data with both NLO calculations and QCD model predictions. Again the NLO predictions reproduce the data whereas at low Q^2 the LEPTO predictions fall below the data and at high Q^2 ARIADNE underestimates the cross section. HERWIG is unable to describe the data everywhere. It should also be noted that the data tends to overshoot the NLO predictions in the lowest ξ bin, which may be an indication that the gluon density has been underestimated in the calculation.

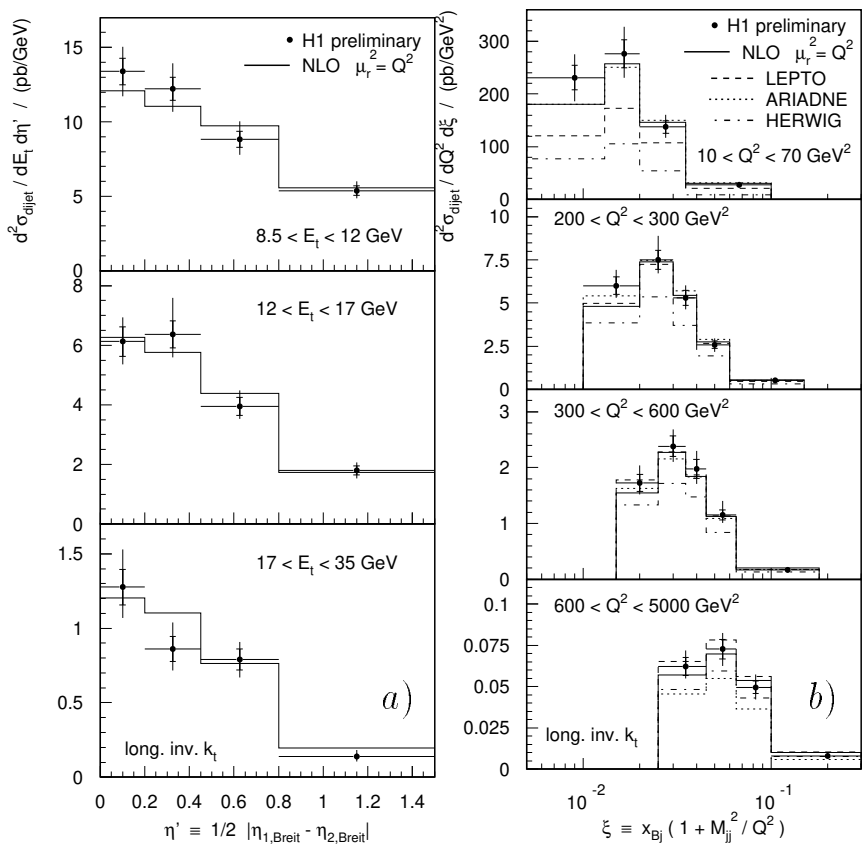

Fig. 3. The doubly differential di-jet cross section a) $d\sigma/dE_t d\eta'$ and b) $d\sigma/dQ^2 d\xi$ compared to the predictions by NLO calculations and QCD models.

The jet cross section can be written as a convolution of perturbative coefficients with the parton densities in the proton.

$$\sigma_{jet} = \sum_n \alpha_S^n [c_{g,n}\, g(x_g, \mu_f) + \sum_f c_{f,n}\, q(x_q, \mu_f)] \tag{7}$$

where the cross section is calculated to all orders in α_S and for all quark flavours f. The perturbative coefficients are denoted $c_{g,n}$ for the gluon and $c_{f,n}$ for the quarks and the parton density functions are written $g(x_g, \mu_f)$ and $q(x_q, \mu_f)$ for the gluon and the quarks, respectively. The formula illustrates the correlation between the strong coupling constant and the parton densities, which prevents an unambigous determination of the gluon density from a deep inelastic measurement alone. In order to circumvent this problem the α_S value of 0.119 ± 0.005 from measurements at LEP [22] was used.

The perturbation coefficients are not all independent but can be reduced to three independent coefficients by linear combinations of the single flavour coefficients.

$$\begin{aligned} c_G &= c_g, \\ c_\Delta &= 3(c_u - c_d), \\ c_\Sigma &= 1/3(4c_d - c_u) \end{aligned} \tag{8}$$

This results in three independent parton densities.

$$\begin{aligned} \Delta(x_p, \mu_f) &= \sum_f e_f^2 (q_f(x_p, \mu_f) + \overline{q}(x_p, \mu_f)) \\ G(x_p, \mu_f) &= g(x_p, \mu_f) \\ \Sigma(x_p, \mu_f) &= \sum_f (q_f(x_p, \mu_f) + \overline{q}(x_p, \mu_f)) \end{aligned} \tag{9}$$

Table 1 summarizes which parton densities contribute to which order in α_S for the inclusive, σ^{incl}, and the di-jet, σ^{dijet}, cross sections, respectively.

Table 1. LO and NLO contributions of the various parton densities to the inclusive and di-jet cross sections, respectively.

	LO	NLO
σ^{incl}	$\Delta(x)$	$\Delta(x), G(x)$
σ^{dijet}	$G(x), \Delta(x)$	$G(x), \Delta(x), \Sigma(x)$

With the value of α_S fixed to 0.119 ± 0.005 a simultaneous fit of the gluon and quark densities in the proton was performed using data both on inclusive DIS and on di-jet production. The Q^2 region for the inclusive data was restricted to $200 < Q^2 < 650 GeV^2$ which is approximately equal to the jet transverse energy squared in the di-jet data. This also motivates a fixed value of $200 GeV^2$ for the factorization scale, μ^2. In this kinematic region the inclusive data constrain the quark density strongly whereas the di-jet data is mainly sensitive to the gluon density. The di-jet events were required to have $Q^2 > 200 GeV^2$ in order to avoid large NLO corrections and hadronisation effects. For the di-jet data fits were made to the double differential cross sections $d\sigma/dQ^2 d\xi$ and $d\sigma/dQ^2 dx_{Bj}$, and for the inclusive data to $d\sigma/dQ^2 dx_{Bj}$ since these are the most sensitive to the x-dependence of the parton densities.

In Fig. 4 the result of the gluon density fit is compared to global fits using parton density parametrizations according to CTEQ4M, MRST and GRV94HO, and to a QCD analysis of the F_2 structure funcion as measured by the H1 collaboration. The direct measurement indicate a somewhat steeper rise with decreasing x_p than the global fits although the results are compatible within the error band. On the other hand the direct measurement is in good agreement with the H1 QCD analysis of F_2. The errors are dominated by the uncertainty in the energy scales of the electromagnetic and hadronic calorimeters, and in the determination of the luminosity.

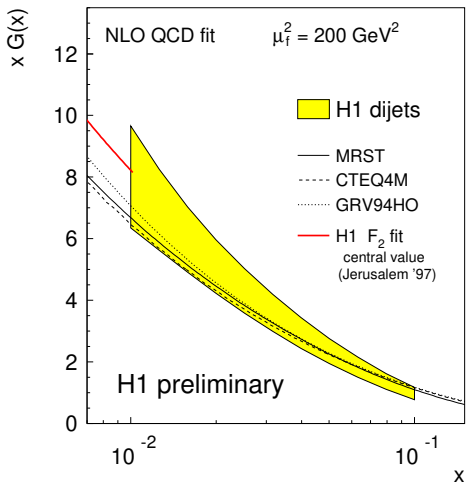

Fig. 4. The gluon density in the proton. The result of the direct determination is compared to global fits with various parton density parametrizations and to a QCD analysis of the proton structure function F_2.

4 A study of differential jet rates

In an H1 analysis differential di-jet rates have been used for comparisons with various QCD models and to NLO predictions. The differential di-jet rate is defined as the number of di-jet events which is obtained with a predefined cut-off value for the resolution parameter, y_{cut}, in the jet algorithm. In an iterative process the jet candidates with the smallest invariant masses are combined until exactly two hard jets remain. The maximum value of the resolution parameter at which two hard jets are resolved is denoted y_2.

The data used for the analysis by H1 were collected in the years 1995-97 and corresponds to an integrated luminosity of $35pb^{-1}$. The events were restricted to the kinematic range $Q^2 > 150GeV^2$ and $0.1 > y > 0.7$ which results in a data sample of 60000 events. The statistics allow a subdivision into three different ranges in Q^2.

Two jet algorithms, the factorizable k_T-algorithm and the modified Durham algorithm, have been used in the study. The k_T-algorithm was applied in the Breit frame with a cut-off value of $y_2 > 0.8$ which approximately corresponds to a mean transverse jet energy of 10 GeV in the Breit frame. The modified Durham algorithm was used in the laboratory system. The resolution parameter was given by $y_2 = k_T^2/W^2$ and the cut-off value was chosen to be $y_2 = 0.005$ which again corresponds to a mean transverse jet energy of 10 GeV in the Breit frame. For both algorithms the jets were restricted to an angular region $10^o < \theta < 140^o$ to ensure good detector acceptance. In addition jets reconstructed below 7^o by the Durham algorithm were rejected.

The di-jet distributions presented have been corrected for detector effects and the influence of QED radiation. The major systematic error comes from the uncertainties in the energy scales of the electromagnetic and hadronic calorimeters.

Data have been compared to the LEPTO and ARIADNE models and to NLO calculations performed with the DISENT program using Q^2 as renormalization scale. The hadronisation effects have been estimated from simulations with the QCD models and were found to be between 10% and 20%.

Fig. 5a shows that the y_2 distributions are in good agreement with both Monte Carlo models and NLO predictions in all three Q^2 bins. The spectra get harder as Q^2 increases. The z_p distributions, however, are not so well described by the models which tend to overshoot the data as seen in Fig. 5b. Again the NLO calculations reproduce the data. In Fig. 6 the distribution of the polar angle for the most forward going jet is plotted and compared to NLO predictions where also the BGF fraction is indicated. At high Q^2, where the BGF fraction is of the order of 30%, the agreement is good whereas in the low Q^2 region, which contains 70% BGF, the NLO calculations seems to fall below the data point in the lowest θ bin. This might indicate an underestimation of the gluon density in the NLO calculation.

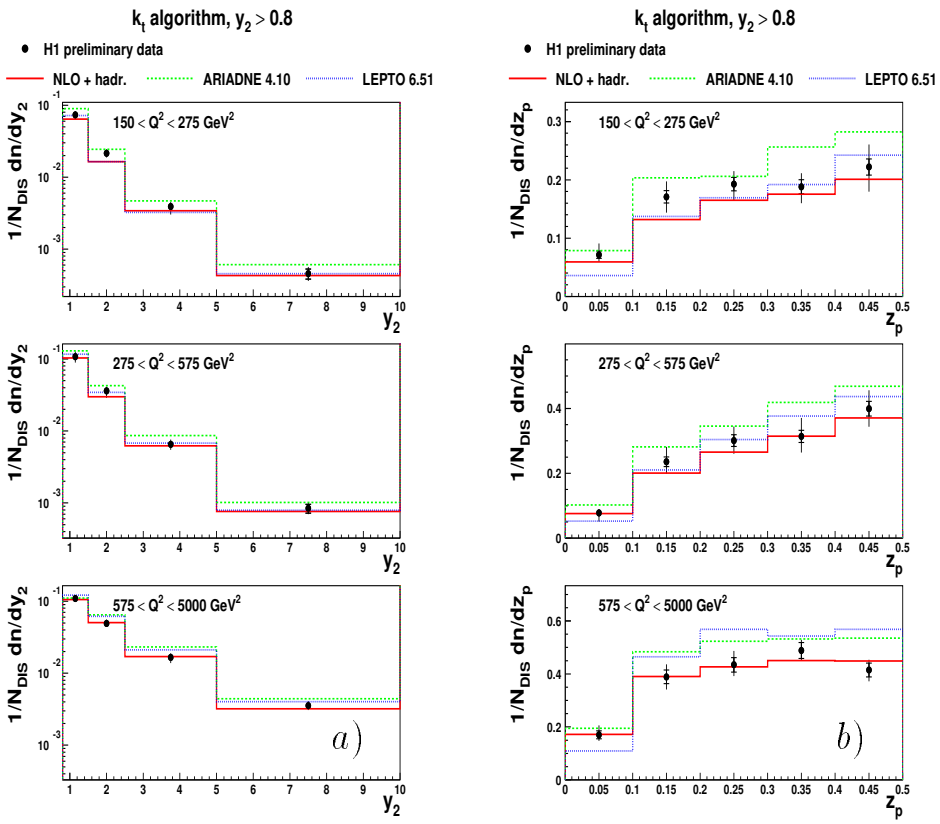

Fig. 5. The differential di-jet rates as a function of a) y_2 and z_p compared to NLO calculations and QCD models.

5 Measurement of the strong coupling constant from di-jet rates

The ZEUS collaboration has used data collected in the years 1996-97 to investigate di-jet rates in deep inelastic scattering with the aim of determining the strong coupling constant, α_S. The data corresponds to an integrated luminosity of 38 pb^{-1}. In order to avoid experimental and theoretical difficulties as far as possible the analysis was performed in the high Q^2 region, $470 < Q^2 < 20000 GeV^2$. The event kinematics was extracted using the double angle method [23] which is the method least sensitive to errors in the absolute energy scale of the calorimeter. It was also proven to be the most accurate one in the Q^2 region investigated.

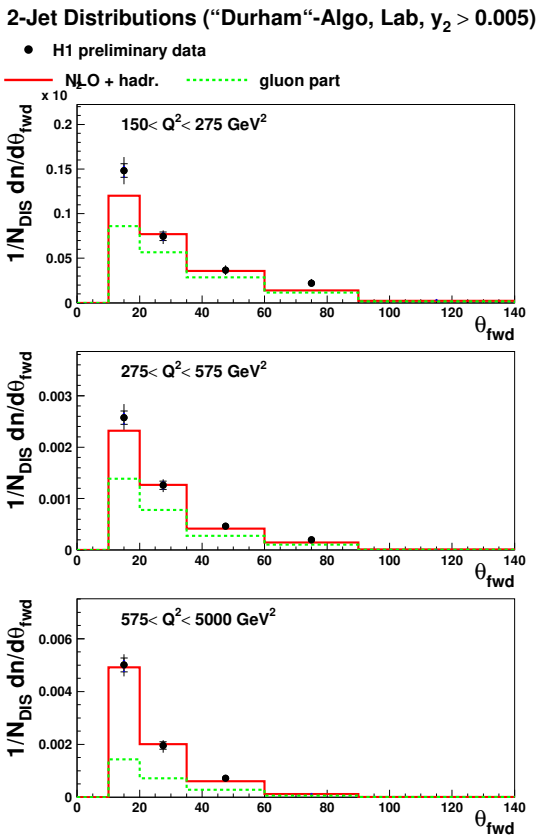

Fig. 6. The distribution in polar angle for the most forward going jet compared to NLO calculations. The contribution from the BGF process is indicated.

The jet reconstruction was performed in the Breit frame using the longitudinally invariant k_T-algorithm. Energy clusters in the calorimeter were used as jet seeds and the jet reconstruction procedure followed the Snowmass scheme. Events with exactly two jets were selected where both jets were required to have energies above 5 GeV and their energy sum to be above 17 GeV. By this cut scenario problems with divergencies, related to soft and collinear gluon emissions, in fixed order calculations can be avoided. In order to ensure that the jets were well inside the acceptance of the detector they were restricted to the rapidity range $-1 < \eta_{LAB} < 2$.

Monte Carlo simulations have been used to correct the data for detector inefficiences and to take effects from QED radiation and hadronisation into account. Further, contributions from Z° exchange had to be included since

the Q^2 range extends as far up as 20000 GeV^2. Comparisons of the data have been made with two versions of the DJANGO program based on the LEPTO and ARIADNE Monte Carlo generators. Also the HERWIG program was selected for comparisons since it uses a different fragmentation algorithm to describe the hadronisation.

For calulations of NLO cross sections the DISENT program was used and it was checked to be consistent with the results of the DISASTER++ program to within a few percent.

Various control plots were produced in order to see how well the data was reproduced by Monte Carlo models and NLO predictions. Fig. 7 shows the differential di-jet cross section as a function of the the transverse energies, E_t, and rapidities, η, of the two jets in the event. The uncertainty due to the hadronic energy scale of the calorimeter is the dominant systematic error. The error bars contain contributions from all other systematic errors and the statistical errors added in quadrature. The NLO calculations have been performed by DISENT in the $\overline{MS}$ renormalization scheme using the parton density parametrization according to CTEQ4M [24] and choosing $\mu_R^2 = \mu_F^2 = Q^2$ as renormalisation and factorization scales. A closer look to the renormalisation scale dependence of the NLO calculations motivates the lower Q^2 cut of 470 GeV^2 above which the dependence is very small. Also the dependence on the parton density functions is small in this region. An excellent agreement between data and NLO calculations is observed in all plots which is a necessary condition for a reliable extraction of the strong coupling constant.

In each Q^2-bin the ratio of di-jet events, $R_{2+1} = \sigma_{2+1}/\sigma_{tot}$, was calculated with the DISENT program. Five different values of the strong coupling constant, ranging from 0.110 to 0.122, were used in the CTEQ4M parametrization of the parton density function but also the MRST parametrization was used for a consistency check. The dijet rates obtained for the five α_S values were fitted with a straight line in each Q^2-bin to allow for a continuous variation of α_S with the di-jet rate. The α_S value was then extracted through a χ^2 fit of the NLO predictions to the measured di-jet ratio according to:

$$\chi^2 = \sum_{i=1}^{5} \frac{(R^i_{2+1,meas} - R^i_{2+1,theor})^2}{\sigma^{2,i}_{2+1}} \tag{10}$$

The value obtained is:

$$\alpha_S = 0.120 \pm 0.003(stat) \tag{11}$$

A summary of the systematic errors are given in Fig. 8. As has been mentioned previously and which is clearly illustrated in the figure, is that the by far dominant systematic error comes from the uncertainty in the jet energy scale. Another contribution to the experimental systematic error is due to the model dependence. The dependences of the renormalization scale, the

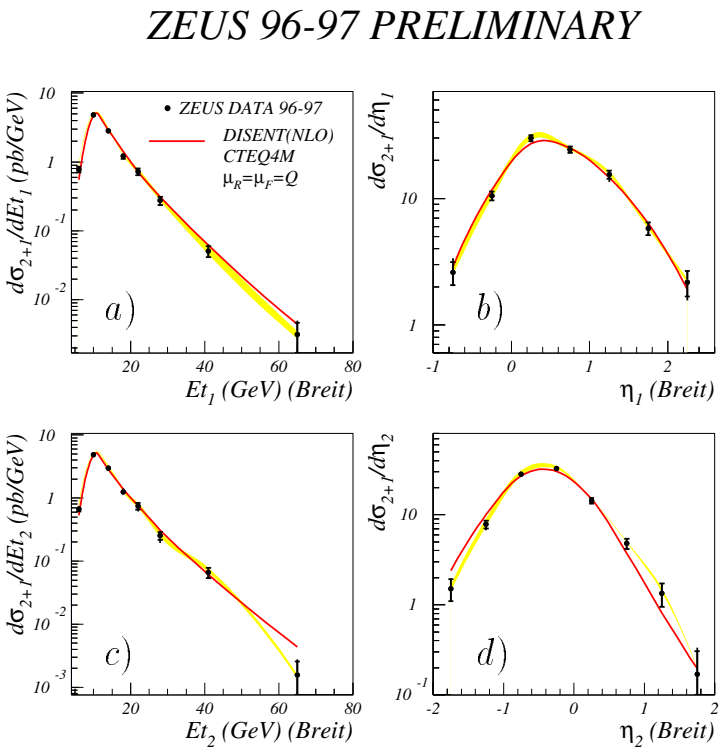

Fig. 7. The di-jet cross sections a) $d\sigma/dE_{t1}$, b) $d\sigma/d\eta_1$), c) $d\sigma/dE_{t2}$ and d) $d\sigma/d\eta_2$ compared to the predictions by NLO calculations.

parton density functions and the NLO program used, define the theoretical systematic error. The final result including all errors is:

$$\alpha_S = 0.120 \pm 0.003(stat) \pm^{0.005}_{0.006} (exp) \pm^{0.002}_{0.003} (th) \qquad (12)$$

5.1 Summary

Jet production in DIS provides an interesting testing ground of perturbative QCD which in many respects offers higher sensitivity and contains more information about the proton structure than the inclusive measurements of the proton structure function. Over the past few years quite some progress has been made in the description of jet production in deep inelastic scattering. Several Monte Carlo programs for calculations of next to leading order α_S jet cross sections have been developed, which allow different jet algorithms to be applied and experimental cuts to be defined. Although the new programs offer quantitative agreement at large Q^2, deviations were observed in the low

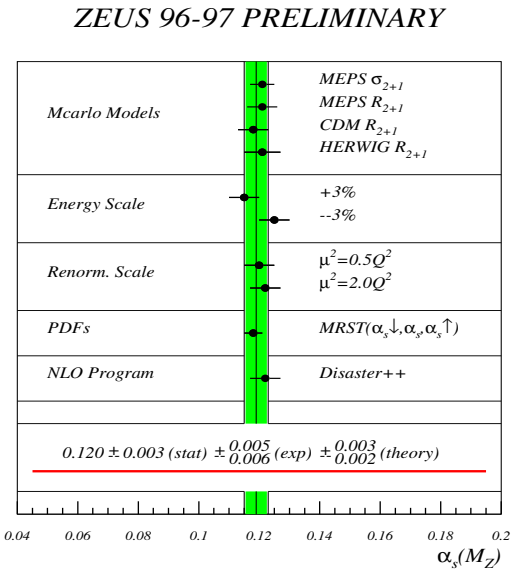

Fig. 8. Contributions to the systematic errors on the measured α_S value.

Q^2 region. Only recently an explanation of these data could be achieved both by a Monte Carlo model [25] and by NLO calculations [26].

5.2 Acknowledgement

This presentation was given on behalf of the H1 and ZEUS collaborations. I would like to thank S. Schlenstedt, L. Sinclair, E. Tasso, M. Weber, N. Tobien and M. Wobisch for providing me with the relevant material.

References

1. E. Mirkes and D. Zeppenfeld, Phys. Lett. B380(1996)205.
2. S. Catani and M. Seymour, Nucl. Phys. B485(1997)291.
3. D. Graudenz, hep-ph/9710244.
4. K. Fabricius, G. Kramer, G. Schierholz and I. Schmitt, Z. Phys. C11(1981)315, G. Kramer and B. Lampe, Fortschr. Phys. 37(1989)161, W.T. Giele and E.W.N. Glover, Phys. Rev. D46(1992)1980, W.T. Giele, E.W.N. Glover and D.A. Kosower, Nucl. Phys. B403(1993)663.
5. R.K. Ellis, D.A. Ross and A.E. Terrano, Nucl.Phys. B178(1981)421.
6. G. Ingelman, in Proc. Workshop on Physics at HERA, Hamburg, October 1991, eds. W. Buchmüller and G. Ingelman, vol. 3(1992)1366. G. Ingelman, A. Edin and J. Rathsman, Comput. Phys. Comm. 101(1997)108.
7. G. Marchesini et al., Comput. Phys. Comm. 67(1997)465.

8. Yu.L. Dokshitzer, Sov. Phys. JETP 46(1977)641, V.N. Gribov and L.N. Lipatov, Sov. J. Nucl. Phys.15(1972)438 and 675, G. Altarelli and G. Parisi, Nucl. Phys. 126(1977)297.
9. L. Lönnblad, Comput. Phys. Comm. 71(1992)15, L. Lönnblad, Z. Phys. C65(1995)285.
10. G. Gustafson, Phys. Lett. B175(1986)453, G. Gustafson and U. Petterson, Nucl. Phys. B306(1988)746, B. Andersson, G. Gustafson, L. Lönnblad and U. Petterson, Z. Phys. C43(1989)625,
11. P. Hoyer et al., Nucl. Phys. B161(1979)349, A. Ali et al., Nucl. Phys. B168(1980)409, A. Ali et al., Phys. Lett. 93B(1980)155.
12. B. Andersson, G. Gustafson, C. Peterson, Z. Phys. C1(1979)105.
13. B.R. Webber, Nucl. Phys.B238(1984)492, G. Marchesini, B.R. Webber, Nucl. Phys. B238(1984)1
14. CDF Collab., F. Abe et al., Phys Rev. Lett. 70(1993)713, M.H. Seymour, Z. Phys. C62(1994)127.
15. S. Catani, Yu.L. Dokshitzer and B.R. Webber, Phys. Lett. B285(1992)291.
16. S.D. Ellis and D.E. Soper, Phys. Rev. D48(1993)3160, S. Catani, Yu. L. Dokshitzer, M.H. Seymour and B.R. Webber, Nucl. Phys. B406(1993)187.
17. JADE Collab., W. Bartel et al., Z. Phys. C61(1986)23.
18. H1 Collab., S. Aid et al., Nucl. Phys. B449(1995)3.
19. K. Charchula, G. Schuler and H. Spiesberger, Comput. Phys. Comm. 81(1994)381.
20. A. Kwiatkowski, H. Spiesberger and H.-J. Möhring, Comp. Phys. Comm. 69(1992)155.
21. H.L. Lai et al., hep-ph/9903282
22. S. Catani, Int.Symposium on Lepton Photon Interactions, Hamburg, Germany (1997) and hep-ph/9712442.
23. S. Bentvelsen, J. Engelen and P. Kooijman, Proc. of the Workshop 'Physics at HERA', vol.1, eds. W. Buchmüller and G. Ingelman, DESY(1991)23.
24. H.L.Lai et al., Phys. Rev. D55(1997)1280.
25. H. Jung, L. Jönsson and H. Küster, DESY 98-051 and hep-ph/9805396, H. Jung, L. Jönsson and H. Küster, hep-ph/9811368 and Proc. of the Workshop 'Photon interactions and the photon structure', eds. G. Jarlskog and T. Sjöstrand, Lund(1998)229, H. Jung, L. Jönsson and H. Küster, Eur. Phys. J. C9(1999)383.
26. G. Kramer and B. Pötter, Eur. Phys. J. C1(1998)261, G. Kramer and B. Pötter, Eur. Phys. J. C5(1998)665, G. Kramer and B. Pötter, Phys. Lett. B453(1999)295.